Inorg. Chem. **2007**, *46*, 2398–2408

Kinetic Analysis of the Conversion of Nonheme (Alkylperoxo)iron(III) Species to Iron(IV) Complexes

Michael P. Jensen,[†,‡] Antoni Mairata i Payeras,[†,§] Adam T. Fiedler,[†] Miquel Costas,[†,∥] József Kaizer,[†,⊥] Audria Stubna,[#] Eckard Münck,*[,#] and Lawrence Que, Jr.*[,†]

Department of Chemistry and the Center for Metals in Biocatalysis, University of Minnesota, Minneapolis, Minnesota 55455, and Department of Chemistry, Carnegie Mellon University, Pittsburgh, Pennsylvania 15213

Received May 8, 2006

Low-spin mononuclear (alkylperoxo)iron(III) complexes decompose by peroxide O–O bond homolysis to form iron(IV) species. We examined the kinetics of previously reported homolysis reactions for (alkylperoxo)iron(III) intermediates supported by TPA (tris(2-pyridylmethyl)amine) in CH_3CN solution and promoted by pyridine *N*-oxide, and by BPMCN (*N*,*N*-bis(2-pyridylmethyl)-*N*,*N*-dimethyl-*trans*-1,2-diaminocyclohexane) in its cis-β configuration in CH_3CN and CH_2Cl_2, as well as for the previously unreported chemistry of TPA and 5-Me_3TPA intermediates in acetone. Each of these reactions forms an oxoiron(IV) complex, except for the β-BPMCN reaction in CH_2Cl_2 that yields a novel (hydroxo)(alkylperoxo)iron(IV) product. Temperature-dependent rate measurements suggest a common reaction trajectory for each of these reactions and verify previous theoretical estimates of a ca. 60 kJ/mol enthalpic barrier to homolysis. However, both the tetradentate supporting ligand and exogenous ligands in the sixth octahedral coordination site significantly perturb the homolyses, such that observed rates can vary over 2 orders of magnitude at a given temperature. This is manifested as a compensation effect in which increasing activation enthalpy is offset by increasingly favorable activation entropy. Moreover, the applied kinetic model is consistent with geometric isomerism in the low-spin (alkylperoxo)iron(III) intermediates, wherein the alkylperoxo ligand is coordinated in either of the inequivalent cis sites afforded by the nonheme ligands.

1. Introduction

Many monooxygenase enzymes utilize a mononuclear iron(II) center in a nonheme ligand environment to activate dioxygen and effect concomitant oxidation or oxygenation of biological substrates.[1] Peroxo intermediates are often cited as mechanistically important intermediates in such processes that break down to form high-valent oxoiron species.[2] Distinct oxoiron(V) and oxoiron(IV) intermediates can be generated respectively by disparate heterolytic and homolytic cleavage of the peroxide O−O bonds (eqs 1, 2).[3,4] In turn, these highly reactive species carry out the substrate oxidations.[5,6]

$$(L)Fe^{III}-OOR \rightarrow (L)\,Fe^{V}=O + RO^{\ominus} \quad (1)$$

$$(L)Fe^{III}-OOR \rightarrow (L)Fe^{IV}=O + RO^{\bullet} \quad (2)$$

$$(L)Fe^{III}-OOR \rightarrow (L)Fe^{II} + ROO^{\bullet} \quad (3)$$

Our laboratory has pursued a modeling approach to this reactivity using small-molecule iron complexes.[7,8] Several

* To whom correspondence should be addressed. E-mail: emunck@cmu.edu (E.M.), que@chem.umn.edu (L.Q.).
† University of Minnesota.
‡ Current address: Department of Chemistry and Biochemistry, Ohio University, Athens, Ohio 45701.
§ Current address: ICREA Researcher at Bayer Polímeros, 43080 Tarragona, Spain.
∥ Current address: Departament de Quimica, Universitat de Girona, 17071 Girona, Spain.
⊥ Current address: Department of Organic Chemistry, University of Pannonia, H-8200 Veszprém, Hungary.
Carnegie Mellon University.

(1) Costas, M.; Mehn, M. P.; Jensen, M. P.; Que, L., Jr. *Chem. Rev.* **2004**, *104*, 939−986.
(2) Girerd, J.-J.; Banse, F.; Simaan, A. J. *Struct. Bonding* **2000**, *97*, 145−177.
(3) MacFaul, P. A.; Ingold, K. U.; Wayner, D. D.; Que, L., Jr. *J. Am. Chem. Soc.* **1997**, *119*, 10594−10598.
(4) Nielsen, A.; Larsen, F. B.; Bond, A. D.; McKenzie, C. J. *Angew. Chem., Int. Ed.* **2006**, *45*, 1602−1606.
(5) Fitzpatrick, P. F. *Biochemistry* **2003**, *42*, 14083−14091.
(6) Bassan, A.; Blomberg, M. R. A.; Siegbahn, P. E. M. *Chem.−Eur. J.* **2003**, *9*, 4055−4067.
(7) Costas, M.; Chen, K.; Que, L., Jr. *Coord. Chem. Rev.* **2000**, *200−202*, 517−544.

10.1021/ic0607787 CCC: $37.00
Published on Web 02/28/2007

nonheme oxoiron(IV) complexes have been characterized;[9−21] these synthetic complexes exhibit weak visible-NIR ligand field bands at ca. 700 nm, a short Fe═O bond on the order of 1.65 Å, and a low-spin ($S = 1$) ground state. Oxoiron(IV) intermediates also have been detected experimentally in the catalytic cycle of the α-keto acid-dependent enzymes taurine: αKG dioxygenase (TauD)[22−25] and prolyl-4-hydroxylase (P4H).[26] In contrast to the synthetic ligands, the 2-His-1-carboxylate facial triad[1,27] environment of the enzyme affords a weaker ligand field and gives rise to a high-spin ($S = 2$) ground state. However, the difference in the spin states involves only the d_{xy} and $d_{x^2-y^2}$ orbitals, and DFT calculations suggest the Fe═O bonding remains highly covalent and is not significantly perturbed.[28,29]

A number of (alkylperoxo)iron(III) complexes have also been generated, primarily by oxidation of synthetic iron(II) complexes with *tert*-butyl hydroperoxide (^{t}BuOOH).[1,2,14,15,21,30−40] These metastable species have been characterized primarily by EPR and resonance Raman spectroscopy,[2] as well as by X-ray absorption spectroscopy.[14] Enzymes with experimentally observable peroxo species include soybean lipoxygenase,[41] superoxide reductase,[42−45] and naphthalene dioxygenase.[46] The synthetic peroxo complexes exhibit either low- ($S = 1/2$) or high-spin ($S = 5/2$) configurations with concomitant effects on reactivity; spectroscopic analysis and theoretical calculations indicate that low-spin species favor FeO−OR bond homolysis (eq 2), whereas the high-spin intermediates undergo Fe−OOR bond homolysis (eq 3).[36,47,48]

Chart 1

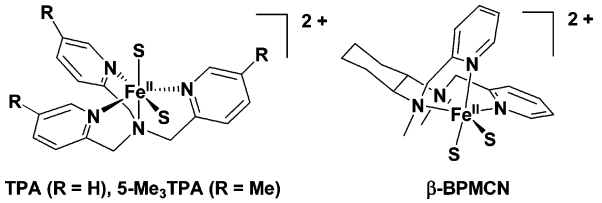

TPA (R = H), 5-Me$_3$TPA (R = Me) β-BPMCN

The TPA and BPMCN ligands (tris(2-pyridylmethyl)amine and *N*,*N*-bis(2-pyridylmethyl)-*N*,*N*-dimethyl-*trans*-1,2-diaminocyclohexane, respectively, Chart 1) support low-spin (alkylperoxo)iron(III) intermediates, and their conversions to oxoiron(IV) species have been directly observed.[15,21,38] This work examines the temperature-dependent kinetics of FeO−OR bond homolyses for the predominantly low-spin (alkylperoxo)iron(III) intermediates supported by these ligands (TPA, 5-Me$_3$TPA, *β*-BPMCN, Chart 1) in various solvents (acetone, CH_3CN, CH_2Cl_2). The reactions produce oxoiron(IV) in all cases, except for the previously reported formation of a novel (hydroxo)(alkylperoxo)iron(IV) product derived from Fe^{II}(*β*-BPMCN)$(OTf)_2$ in CH_2Cl_2.[15] Nevertheless, some mechanistic similarities were observed in formation of this

(8) Shan, X.; Que, L., Jr. *J. Inorg. Biochem.* **2006**, *100*, 421−433.
(9) Grapperhaus, C. A.; Mienert, B.; Bill, E.; Weyhermüller, T.; Wieghardt, K. *Inorg. Chem.* **2000**, *39*, 5306−5317.
(10) Rohde, J.-U.; In, J.-H.; Lim, M. H.; Brennessel, W. W.; Bukowski, M. R.; Stubna, A.; Münck, E.; Nam, W.; Que, L., Jr. *Science* **2003**, *299*, 1037−1039.
(11) Lim, M. H.; Rohde, J.-U.; Stubna, A.; Bukowski, M. R.; Costas, M.; Ho, R. Y. N.; Münck, E.; Nam, W.; Que, L., Jr. *Proc. Natl. Acad. Sci. U.S.A.* **2003**, *100*, 3665−3670.
(12) Kaizer, J.; Klinker, E. J.; Oh, N. Y.; Rohde, J.-U.; Song, W. J.; Stubna, A.; Kim, J.; Münck, E.; Nam, W.; Que, L., Jr. *J. Am. Chem. Soc.* **2004**, *126*, 472−473.
(13) Balland, V.; Charlot, M.-F.; Banse, F.; Girerd, J.-J.; Mattioli, T. A.; Bill, E.; Bartoli, J.-F.; Battioni, P.; Mansuy, D. *Eur. J. Inorg. Chem.* **2004**, 301−308.
(14) Rohde, J.-U.; Torelli, S.; Shan, X.; Lim, M. H.; Klinker, E. J.; Kaizer, J.; Chen, K.; Nam, W.; Que, L., Jr. *J. Am. Chem. Soc.* **2004**, *126*, 16750−16761.
(15) Jensen, M. P.; Costas, M.; Ho, R. Y. N.; Kaizer, J.; Mariata i Payeras, A.; Münck, E.; Que, L., Jr.; Rohde, J.-U.; Stubna, A. *J. Am. Chem. Soc.* **2005**, *127*, 10512−10525.
(16) Bukowski, M. R.; Koehntop, K. D.; Stubna, A.; Bominaar, E. L.; Halfen, J. A.; Münck, E.; Nam, W.; Que, L., Jr. *Science* **2005**, *310*, 1000−1002.
(17) Klinker, E. J.; Kaizer, J.; Brennessel, W. W.; Woodrum, N. L.; Cramer, C. J.; Que, L., Jr. *Angew. Chem., Int. Ed.* **2005**, *44*, 3690−3694.
(18) Kim, S. O.; Sastri, C. V.; Seo, M. S.; Kim, J.; Nam, W. *J. Am. Chem. Soc.* **2005**, *127*, 4178−4179.
(19) Sastri, C. V.; Park, M. J.; Ohta, T.; Jackson, T. A.; Stubna, A.; Seo, M. S.; Lee, J.; Kim, J.; Kitagawa, T.; Münck, E.; Que, L., Jr.; Nam, W. *J. Am. Chem. Soc.* **2005**, *127*, 12494−12495.
(20) Suh, Y.; Seo, M. S.; Kim, K. M.; Kim, Y. S.; Jang, H. G.; Tosha, T.; Kitagawa, T.; Kim, J.; Nam, W. *J. Inorg. Biochem.* **2006**, *100*, 627−633.
(21) Paine, T. K.; Costas, M.; Kaizer, J.; Que, L., Jr. *J. Biol. Inorg. Chem.* **2006**, *11*, 272−276.
(22) Price, J. C.; Barr, E. W.; Tirupati, B.; Bollinger, J. M., Jr.; Krebs, C. *Biochemistry* ***2003***, *42*, 7497−7508.
(23) Price, J. C.; Barr, E. W.; Glass, T. E.; Krebs, C.; Bollinger, J. M., Jr. *J. Am. Chem. Soc.* **2003**, *125*, 13008−13009.
(24) Proshlyakov, D. A.; Henshaw, T. F.; Monterosso, G. R.; Ryle, M. J.; Hausinger, R. P. *J. Am. Chem. Soc.* **2004**, *126*, 1022−1023.
(25) Riggs-Gelasco, P. J.; Price, J. C.; Guyer, R. B.; Brehm, J. H.; Barr, E. W.; Bollinger, J. M., Jr.; Krebs, C. *J. Am. Chem. Soc.* **2004**, *126*, 8108−8109.
(26) Hoffart, L. M.; Barr, E. W.; Guyer, R. B.; Bollinger, J. M., Jr.; Krebs, C. *Proc. Natl. Acad. Sci. U.S.A.* **2006**, *103*, 14738−14743.
(27) Que, L., Jr. *Nat. Struct. Biol.* **2000**, *7*, 182−184.
(28) Decker, A.; Rohde, J.-U.; Que, L., Jr.; Solomon, E. I. *J. Am. Chem. Soc.* **2004**, *126*, 5378−5379.
(29) Pestovsky, O.; Stoian, S.; Bominaar, E. L.; Shan, X.; Münck, E.; Que, L., Jr.; Bakac, A. *Angew. Chem., Int. Ed.* **2005**, *44*, 6871−6874.
(30) Ménage, S.; Wilkinson, E. C.; Que, L., Jr.; Fontecave, M. *Angew. Chem., Int. Ed.* **1995**, *34*, 203−205.
(31) Kim, J.; Larka, E.; Wilkinson, E. C.; Que, L., Jr. *Angew. Chem., Int. Ed.* **1995**, *34*, 2048−2051.
(32) Zang, Y.; Kim, J.; Dong, Y.; Wilkinson, E. C.; Appelman, E. H.; Que, L., Jr. *J. Am. Chem. Soc.* **1997**, *119*, 4197−4205.
(33) Wada, A.; Ogo, S.; Watanabe, Y.; Mukai, M.; Kitagawa, T.; Jitsukawa, K.; Masuda, H.; Einaga, H. *Inorg. Chem.* **1999**, *38*, 3592−3593.
(34) Ogihara, T.; Hikichi, S.; Akita, M.; Uchida, T.; Kitagawa, T.; Moro-oka, Y. *Inorg. Chim. Acta* **2000**, *297*, 162−170.
(35) Sobolev, A. P.; Babushkin, D. E.; Talsi, E. P. *J. Mol. Catal., A* **2000**, *159*, 233−245.
(36) Kim, J.; Zang, Y.; Costas, M.; Harrison, R. G.; Wilkinson, E. C.; Que, L., Jr. *J. Biol. Inorg. Chem.* **2001**, *6*, 275−284.
(37) Jensen, M. P.; Lange, S. J.; Mehn, M. P.; Que, E. L.; Que, L., Jr. *J. Am. Chem. Soc.* **2003**, *125*, 2113−2128.
(38) Kaizer, J.; Costas, M.; Que, L., Jr. *Angew. Chem., Int. Ed.* **2003**, *42*, 3671−3673.
(39) Lehnert, N.; Fujisawa, K.; Solomon, E. I. *Inorg. Chem.* **2003**, *42*, 469−481.
(40) Bautz, J.; Comba, P.; Que, L., Jr. *Inorg. Chem.* **2006**, *45*, 7077−7082.
(41) Skrzypczak-Jankun, E.; Bross, R. A.; Carroll, R. T.; Dunham, W. R.; Funk, M. O., Jr. *J. Am. Chem. Soc.* **2001**, *123*, 10814−10820.
(42) Coulter, E. D.; Emerson, J. P.; Kurtz, D. M., Jr.; Cabelli, D. E. *J. Am. Chem. Soc.* **2000**, *122*, 11555−11556.
(43) Emerson, J. P.; Coulter, E. D.; Cabelli, D. E.; Phillips, R. S.; Kurtz, D. M., Jr. *Biochemistry* **2002**, *41*, 4348−4357.
(44) Mathé, C.; Mattioli, T. A.; Horner, O.; Lombard, M.; Latour, J.-M.; Fontecave, M.; Nivière, V. *J. Am. Chem. Soc.* **2002**, *124*, 4966−4967.
(45) Nivière, V.; Asso, M.; Weill, C. O.; Lombard, M.; Guigliarelli, B.; Favaudon, V.; Houée-Levin, C. *Biochemistry* **2004**, *43*, 808−818.
(46) Karlsson, A.; Parales, J. V.; Parales, R. E.; Gibson, D. T.; Eklund, H.; Ramaswamy, S. *Science* **2003**, *299*, 1039−1042.
(47) Lehnert, N.; Ho, R. Y. N.; Que, L., Jr.; Solomon, E. I. *J. Am. Chem. Soc.* **2001**, *123*, 8271−8290.
(48) Lehnert, N.; Ho, R. Y. N.; Que, L., Jr.; Solomon, E. I. *J. Am. Chem. Soc.* **2001**, *123*, 12802−12816.

Table 1. Spectroscopic Data for Decomposition Reactions of (Alkylperoxo)iron(III) Intermediates to Iron(IV) Species

complex	solvent	T (K)	other additive	$Fe^{III}-OO^tBu$ LMCT, λ_{max}, nm (ϵ_{obs})	$Fe^{III}-OO^tBu$ mole fraction	$Fe^{IV}=O$ LF, λ_{max}, nm (ϵ_{obs})	Fe^{IV} mole fraction	ref
Fe(5-Me$_3$TPA)	acetone	228		560 (900)		746 (160)		*a*
Fe(5-Me$_3$TPA)	acetone	213		560 (1500)	0.72[b]			*a*
Fe(TPA)	MeCN	231	PyO (10 mM)	593 (2100)		746 (340)	0.95[b]	38
Fe(BPMCN)	MeCN	228	H_2O (300 mM)	600 (2200)		753 (280)	0.90[b]	15
Fe(BPMCN)	CH_2Cl_2	206		566 (2200)	0.86[c]	*d*	0.94(3)[e]	15

[a] This work. [b] Determined by Mössbauer spectroscopy. [c] Determined by EPR spectroscopy. [d] Product is an (alkylperoxo)iron(IV) complex. [e] Determined by NMR spectroscopy.

distinct product, and theoretical predictions about the common O−O bond homolyses were tested experimentally.

2. Experimental Section

Synthetic and general experimental procedures were described previously.[15,21,38,49] Electronic absorption spectra were recorded on a Hewlett-Packard (Agilent) 8452 diode array spectrophotometer over a 190−1100 nm range in quartz cuvettes cooled to the desired temperature either in a liquid-nitrogen cryostat (Unisoku) or in a methanol-filled dewar fitted with quartz windows placed in the optical path and cooled by a closed loop of chilled methanol from a circulating bath equipped with an immersion cooler under control of a thermostat (Neslab). Global kinetic fits were carried out using SPECFIT (Spectrum Software Associates, Chapel Hill, NC)[50] on optical datasets truncated to remove initial iron(II) oxidation and terminal quenching of metastable iron(IV) products. X-band EPR spectra were obtained at 2 K on a Bruker E-500 spectrometer equipped with an Oxford ESR-10 liquid-helium cryostat. Resonance Raman spectra were collected on an Acton AM-506 spectrometer (2400-groove grating) using Kaiser Optical holographic super-notch filters with a Princeton Instruments liquid-N_2-cooled (LN-1100PB) CCD detector with 4 or 2 cm^{-1} spectral resolution. Spectra were obtained using a back-scattering geometry on liquid-N_2 frozen samples with laser excitation from either a Spectra Physics 2030 argon ion laser and a 375B CW dye (Rhodamine 6G) or a Spectra Physics Beamlock 2060 krypton laser. Raman frequencies were referenced to indene.

3. Results

General Remarks. (Alkylperoxo)iron(III) intermediates supported by TPA, 5-Me$_3$-TPA, and BPMCN ligands (Chart 1) are formed by treatment of iron(II) precursors with excess ^{t}BuOOH in various solvents (acetone, CH_3CN, CH_2Cl_2).[15,32,38] These complexes possess intense LMCT bands ($\epsilon = 2000-2500$ M^{-1} cm^{-1}) and convert to metastable oxo- or (alkylperoxo)iron(IV) species in near-quantitative yields (Table 1). In this work, decay of the (alkylperoxo)iron(III) intermediates was monitored by visible−NIR spectroscopy, and analysis of their reaction kinetics revealed common mechanistic features among the disparate reactions. Consistent with the observed extinctions, optical data were obtained from reactions carried out using millimolar concentrations of iron(II) precursors and the minimal excess of ^{t}BuOOH empirically determined to generate optimal yields of (alkylperoxo)iron(III) species (i.e., 2 equiv in CH_3CN, 5−10 equiv in CH_2Cl_2, and 10 equiv in acetone, added as a concentrated stock solution, 5.5 M in nonane); conversion was found to be nearly quantitative as judged by EPR and Mössbauer spectra, except in acetone.

The initial oxidation of iron(II) exhibited complex kinetic behavior plausibly associated with autocatalysis (Figures S1 and S2 in Supporting Information); observed reaction velocities were roughly proportional to initial concentrations of iron(II) and ^{t}BuOOH, but detailed mechanistic analysis of this step is ongoing and will be addressed in a future manuscript. Nonetheless, monotonic accumulation of the (alkylperoxo)iron(III) CT chromophore continued until iron(II) was exhausted, and then subsequent decay to iron(IV) abruptly commenced. Therefore, the (alkylperoxo)iron(III) decay was cleanly separable from both the preceding rapid accumulation phase (Figures S3 and S4 in Supporting Information), as well as from the slow terminal quenching of metastable iron(IV) product. At reaction temperatures of ca. 228 K, the accumulation phase persisted for 2−5 min in CH_3CN, tens of seconds in acetone, and seconds in CH_2Cl_2.

Kinetics of the subsequent alkylperoxoiron(III) decay phase(s) to iron(IV) were modeled by assuming first-order kinetics for all observed phases and using global least-squares techniques. Unless otherwise noted, we have assumed irreversible unimolecular O−O bond homolyses as the rate-limiting steps, eq 2, yielding the rate law of eq 4, where we take $k_{obs} = k$ of reaction 2.[51]

$$-d[\{Fe^{III}(L)OOR\}^{2+}]/dt = d[\{(L)Fe^{IV}{=}O\}^{2+}]/dt = -k_{obs}[\{Fe^{III}(L)OOR\}^{2+}] \quad (4)$$

Our interpretation of the kinetic results in this study thus depends on the assumed validity of this equation. Demonstration of the independence of k_{obs} on ^{t}BuOOH concentration

(49) Mairata i Payeras, A.; Ho, R. Y. N.; Fujita, M.; Que, L., Jr. *Chem.—Eur. J.* **2004**, *10*, 4944−4953.
(50) Maeder, M.; Zuberbühler, A. D. *Anal. Chem.* **1990**, *62*, 2220−2224.
(51) Trapping of the reactive ^{t}BuO$^\bullet$ byproduct was further considered. This radical can decay either by β-scission to form acetone and $CH_3^\bullet$ or by H-atom abstraction from solvent and excess ^{t}BuOOH to form relatively unreactive alkylperoxyl radicals, ^{t}BuOO$^\bullet$ decomposing in turn to O_2 and stable ^{t}BuOO^{t}Bu. Comparable rates for these processes are expected at room temperature (e.g., 6×10^4 s^{-1} and 1×10^7 M^{-1} s^{-1} for β-elimination and H-atom abstraction from ^{t}BuOOH, respectively in CH_3CN).[52−55] However, the reaction barrier to bimolecular H-atom abstraction is expected to be largely entropic,[56] whereas unimolecular β-scission exhibits a relatively favorable activation entropy and a largely enthalpic barrier.[54,55] So the bimolecular decay pathway is expected to dominate trapping at the lower temperatures used in this study. This notion is corroborated by reaction of [Fe^{II}(β-BPMCN)](OTf)$_2$ with $(CD_3)_3COOH$ in CH_2Cl_2 at −77 °C; integrity of the ^{t}Bu-d_9 substituent during the course of the reaction was demonstrated, as the resonance of acetone-d_6 was not observed by ^2H NMR spectroscopy.[15]
(52) Paul, H.; Small, R. D., Jr.; Scaiano, J. C. *J. Am. Chem. Soc.* **1978**, *100*, 4520−4527.
(53) Snelgrove, D. W.; Lusztyk, J.; Banks, J. T.; Mulder, P.; Ingold, K. U. *J. Am. Chem. Soc.* **2001**, *123*, 469−477.

Table 2. Spectroscopic Characterization of (Alkylperoxo)iron(III) Species

$[Fe(L)(OO^tBu)(X)]^{2+}$ complex: L =	solvent	spin state *S*	UV−vis, nm	resonance Raman, cm^{-1} $\delta(^tBu)$	ν(Fe−O)	ν(OO)	ref
TPA (X = NCMe)	CH_3CN	1/2	600	490	696	796	32
6-Me_3-TPA (no X)	CH_3CN	5/2	562	468	637	842,877	32
TPA (X = PyO)	CH_3CN	1/2	593				38
TPA (X = acetone)	acetone	1/2	560	489	693	788	*a*
5-Me_3-TPA (X = acetone)	acetone	1/2	560	488	691	789	*a*
β-BPMCN (X = NCMe or H_2O)	CH_3CN	1/2	600	490	685	793	15
β-BPMCN (X = OTf and/or ROOH?)	CH_2Cl_2	1/2 (minor)	566		680	789	15
		5/2 (major)		474	628, 637, 647, 653	832, 851, 883	15

[a] This work.

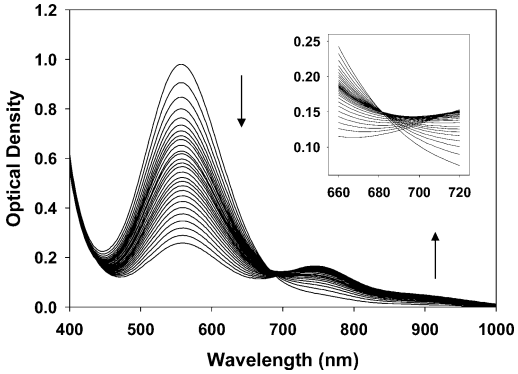

Figure 1. Time-dependent evolution visible−NIR absorption for decay of the (alkylperoxo)iron(III) intermediate supported by 5-Me_3TPA to oxoiron(IV) in acetone at 228 K ($[Fe^{II}]_0 = 1.1$ mM, $[^tBuOOH]_0 = 11$ mM).

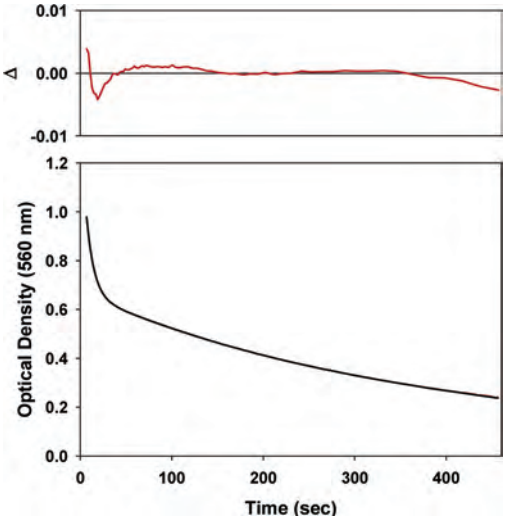

Figure 2. Observed (black) vs calculated (red) optical density at 560 nm for conversion of 5-Me_3TPA-supported (alkylperoxo)iron(III) to oxoiron(IV) shown in Figure 1.

was significantly hindered by complications arising from the initial iron(II) oxidation and side reactions of excess ^{t}BuOOH with products from reaction 2, eqs 5 and 6.[3,51] However, independence of k_{obs} on iron concentration was observed for the decay of the TPA-supported (alkylperoxo)iron(III) intermediate in acetone at −50 °C and for the decay of the BPMCN-supported (alkylperoxo)iron(III) intermediate in CH_2Cl_2 at −67 °C (see Table S1 in Supporting Information), thereby supporting the validity of eq 4.

$$(L)Fe^{IV}{=}O + HOOR \rightarrow (L)Fe^{III}{-}OH + ROO^{\bullet} \quad (5)$$

$$RO^{\bullet} + HOOR \rightarrow ROO^{\bullet} + ROH \quad (6)$$

Decay of $[Fe^{III}(TPA)(OO^tBu)]^{2+}$ and $[Fe^{III}(5\text{-}Me_3TPA)(OO^tBu)]^{2+}$ in Acetone. Treatment of either $[Fe^{II}(TPA)(OTf)_2]$ or $[Fe^{III}(5\text{-}Me_3TPA)(OO^tBu)]^{2+}$ with 10 equiv of ^{t}BuOOH in acetone solution at 228 K resulted in rapid formation of an LMCT band ($\lambda_{max} = 560$ nm, Table 1 and Figure 1) and low-spin iron(III) EPR and Raman spectra (Table 2, Figure S5), analogous to those reported previously for $[Fe^{III}(TPA)(OO^tBu)(NCMe)]^{2+}$ in CH_3CN (vide infra). The LMCT band in acetone is relatively blue-shifted, presumably due to replacement of MeCN with acetone, and its absorbance is lower than expected for full formation of the intermediate, given the molar extinction coefficients typical for such complexes ($\epsilon \sim 2000$ M^{-1} cm^{-1}). Indeed, conversion to the (alkylperoxo)iron(III) species is highly temperature dependent and favored at lower temperature. A Mössbauer spectrum obtained with a frozen sample prepared at 213 K from the addition of 10 equiv of ^{t}BuOOH to a 1.67 mM $[Fe^{II}(5\text{-}Me_3\text{-}TPA)(OTf)_2]$ solution in acetone ($A_{560} = 2.5$) shows 72% of the iron in the sample corresponding to the expected low-spin iron(III) center, with remaining components associated with a high-spin iron(III) center (20%) and a low-spin iron(IV) center (<10%) (Figure S6). If it is assumed that the low-spin (alkylperoxo)iron(III) intermediate contributes almost all of the absorbance at 560 nm, a molar extinction coefficient of 2100 M^{-1} cm^{-1} is calculated, which is fully consistent with previous work (Table 1), so the remaining components are essentially transparent in this region. This initial oxidation product is accordingly formulated as a six-coordinate solvated complex dication $[Fe^{III}(L)(acetone)(OO^tBu)]^{2+}$, L = TPA or 5-$Me_3$-TPA.

Subsequent decay of the 5-Me_3TPA-supported intermediate yielded a ligand field chromophore ($\lambda_{max} = 746$ nm) consistent with its proportional conversion to an oxoiron(IV) complex (Figure 1). However, this reaction failed to conform to simple exponential kinetics, clearly exhibiting two distinct phases for decay of the LMCT band (Figure 2), as well as growth of the ligand field band (Figure S7 in Supporting Information). An isosbestic point initially observed at 682 nm between the bleaching LMCT and growing ligand field chromophores shifted to 716 nm as the decomposition progressed (Figure 1 inset); furthermore, the tailing

(54) Tsentalovich, Y. P.; Kulik, L. V.; Gritsan, N. P.; Yurkovskaya, A. V. *J. Phys. Chem. A* **1998**, *102*, 7975−7980.
(55) Weber, M.; Fischer, H. *J. Am. Chem. Soc.* **1999**, *121*, 7381−7388.
(56) Finn, M.; Friedline, R.; Suleman, N. K.; Wohl, C. J.; Tanko, J. M. *J. Am. Chem. Soc.* **2004**, *126*, 7578−7584.

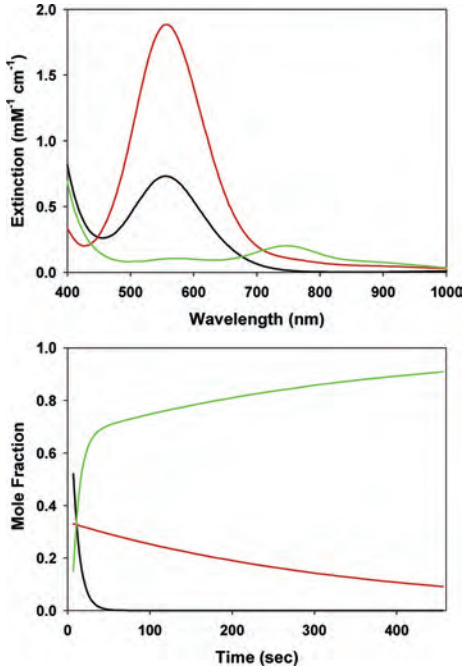

Figure 3. Calculated spectra (top) and time-dependent concentrations (bottom) for an A (red) → C (green), B (blue) → C (green) kinetic model applied to time-dependent optical data shown in Figure 1 for conversion of 5-Me$_3$TPA-supported (alkylperoxo)iron(III) to oxoiron(IV) in acetone at 228 K, with initial mole fractions arbitrarily set to $[A]_0 = 0.52$, $[B]_0 = 0.33$, and $[C]_0 = 0.15$.

absorption of UV-active $\pi-\pi^*$ bands also shifted, and a second isosbestic point eventually developed on the shoulder of the high-energy bands at 437 nm. Both the time-dependent optical data observed at 690 nm between the shifting isosbestic points and at 410 nm on the high-energy tail above the late-developing second isosbestic point clearly exhibited biphasic kinetics of opposing directions (Figures S8 and S9 in Supporting Information). Accordingly, the data were globally fit to double exponential models ($k_{obs} = 1.18(2) \times 10^{-1}$ s^{-1}, $2.86(6) \times 10^{-4}$ s^{-1}; Table S1 and Figure S10 in Supporting Information), with rapid convergence of the least-squares refinement to milli-au residuals (Figure 2 and Figure S11 in Supporting Information).

A parallel, convergent reaction scheme (i.e., A → C, B → C, Figure 3) suggests that the 560 nm LMCT feature is a superposition of two bands that bleach at different rates to form the oxoiron(IV) ligand field spectrum. The LMCT absorption can be partitioned between a continuum of mole fractions representing A and B with concordant effects on their relative extinctions. However, inspection of the 560 nm decay trace clearly shows the fast phase comprises only one-third of the total amplitude (Figure 2). Degenerate sequential models (i.e., A → B → C) must also exist (Figure S12 in Supporting Information),[57] but the calculated intermediate ("B") spectrum contains both (alkylperoxo)iron(III) LMCT and oxoiron(IV) ligand field absorption features, and the former is inverted for one permutation of the observed rates. Hence, we take the sequential model to be nonsensical.

Completely analogous results were obtained for the TPA-supported intermediate (Figures S13−S17 in Supporting Information), although the observed rates decreased slightly ($k_{obs} = 3.17(2) \times 10^{-2}$ s^{-1}, $9.5(1) \times 10^{-4}$ s^{-1} at 223 K). Furthermore, variation of the initial iron and ^{t}BuOOH concentrations by a factor of 4 gave rate constants that were independent of these concentrations (Table S1). These results support our assumption that the decay of the (alkylperoxo)-iron(III) intermediate is a first-order process (eq 4).

Despite the successful fitting of parallel first-order reactions to the optical data, the presence of a significant fraction of the charged iron in an unreactive and spectroscopically transparent state that forms during the initial oxidation of the starting iron(II) complex (Table 1) may raise concern that the complicated observed kinetics might arise from the presence of this mass balance. However, the various isosbestic points observed during decay of the (alkylperoxo)-iron(III) species strongly suggest that this side product is fully inert. To test the generality of our kinetic analysis, we reexamined the previously reported reactions of (alkylperoxo)iron(III) intermediates supported by β-BPMCN in CH_3CN solution,[15] as well as TPA in CH_3CN assisted by added pyridine *N*-oxide,[38] which produce much higher LMCT extinctions and yield oxoiron(IV) in essentially quantitative yield as demonstrated by Mössbauer spectroscopy (Table 1). As described in the following sections, we found evidence of comparable kinetic behavior for these reactions as well.

Decay of [Fe^{III}(TPA)(OO^{t}Bu)]$^{2+}$ in MeCN. [Fe^{II}(TPA)-(NCMe)$_2$]$^{2+}$ reacts with excess ^{t}BuOOH in MeCN solvent at −42 °C to form an intensely blue metastable $S = 1/2$ Fe^{III}−OO^{t}Bu intermediate with λ_{max} at 593 nm (Table 1). As previously reported, conversion of [Fe^{III}(TPA)(OO^{t}Bu)]$^{2+}$ to oxoiron(IV) in CH_3CN solution was sluggish, preventing accumulation of the metastable product. However, fast conversion to a nearly quantitative yield of oxoiron(IV) was obtained upon addition of pyridine *N*-oxide to the preformed (alkylperoxo)iron(III) intermediate at 231 K, which was postulated to bind to the (alkylperoxo)iron(III) species as the sixth ligand, promoting relatively rapid O−O bond homolysis.[38] Decay of the (alkylperoxo)iron(III) LMCT band in the presence of 10 mM pyridine *N*-oxide ($\lambda_{max} = 593$ nm, $\epsilon = 2100$ M^{-1} cm^{-1}) was coincident with the appearance of a ligand field band, indicative of the formation of [Fe^{IV}(O)-(TPA)(pyO)]$^{2+}$ ($\lambda_{max} = 746$ nm, $\epsilon = 340$ M^{-1} cm^{-1}, Figure 4).

Decay of the LMCT absorption proceeds with an apparent isosbestic point near 730 nm (Figure 4), and these optical data were previously fit to first-order observed reaction kinetics using initial rate techniques.[38] In fact, we reconfirmed that the optical data can be fit to a simple exponential decay (A → B), either using a single wavelength coincident with the absorption maximum ($k_{obs} = 1.29(1) \times 10^{-1}$ s^{-1}, $R^2 = 0.9991$) or globally ($k_{obs} = 1.32(1) \times 10^{-1}$ s^{-1}, $\sigma = 1.08 \times 10^{-2}$, Figure 5). However, in both cases the exponential fits showed significant structured residuals. Close inspection of the optical data revealed the apparent isosbestic point again shifted during the reaction (Figure 4 inset), and optical density changes over the bracketed wavelength interval were biphasic (Figure S20 in Supporting Information). These observations closely resembled the spectroscopic results

(57) Vajda, S.; Rabitz, H. *J. Phys. Chem.* **1988**, *92*, 701−707.

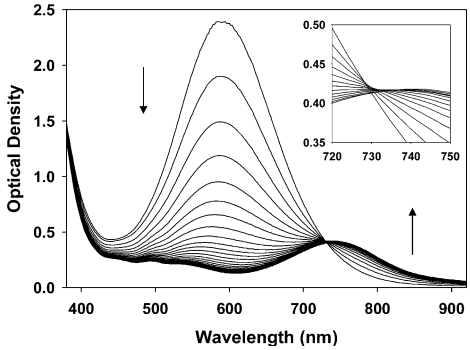

Figure 4. Time-dependent evolution visible-NIR absorption for decay of the (alkylperoxo)iron(III) intermediate supported by TPA to oxoiron(IV) in CH_3CN with added pyridine *N*-oxide at 228 K ($[Fe^{II}]_0$ = 1.3 mM, $[^tBuOOH]_0$ = 2.6 mM, [PyNO] = 10 mM).

obtained in acetone (vide supra), although the red-shift of the LMCT band in CH_3CN nearly disguised the more complex kinetics. Fitting of a parallel A → C, B → C model resulted in significant attenuation and randomization of the residuals (Figure 5 and Figures S18 and S19 in Supporting Information). Calculated spectra for species A and B again featured coincident (alkylperoxo)iron(III) LMCT features; arbitrary assignment of a 1:1 mixture led to approximately degenerate calculated extinctions (Figure 6). Moreover, calculated rates (k_{obs} = 2.5(2) × 10^{-1} s^{-1}, 1.02(3) × 10^{-1} s^{-1}, σ = 4.42 × 10^{-3}) differ by a factor less than 2 about a single-exponential fit, which further conceals the kinetic complexity.

Decay of [Fe^{III}(β-BPMCN)(OO^tBu)]$^{2+}$ in CH_3CN. We recently reported the reaction chemistry of (alkylperoxo)-iron(III) intermediates supported by the BPMCN ligand in its cis-β topology.[15] Interestingly, this chemistry exhibited a marked solvent dependence, with distinct decomposition reactions forming an oxoiron(IV) complex in CH_3CN and a (hydroxo)(alkylperoxo)iron(IV) complex in CH_2Cl_2 (Figure 7), both in essentially quantitative yields as demonstrated by Mössbauer spectroscopy. EPR and Raman spectral characterization of the (alkylperoxo)iron(III) intermediates revealed two overlapping low-spin signals in organonitrile solvents but significant crossover to a mixture of high-spin species in CH_2Cl_2 (Table 2). Kinetic analyses of time-dependent visible−NIR spectrophotometric data for conversion of the (alkylperoxo)iron(III) intermediates to the disparate iron(IV) products were undertaken to gain insight into the solvent-dependent decay mechanisms.

Spectra obtained during decay of the (alkylperoxo)iron-(III) intermediate to an oxoiron(IV) species at 228 K in CH_3-CN resembled the TPA reaction (Figure 7A). For this reaction, it was necessary to introduce 0.3 mM H_2O to accelerate the initial oxidation of iron(II), presumably converting the kinetically inert low-spin [Fe^{II}(BPMCN)-$(NCMe)_2$]$^{2+}$ precursor to the more labile high-spin [Fe^{II}-$(BPMCN)(OH_2)_2$]$^{2+}$; therefore, the obtained (alkylperoxo)-iron(III) species might have retained an aqua ligand in the sixth site. An intense LMCT chromophore centered at 600 nm (ϵ = 2200 M^{-1} cm^{-1}) bleached monotonically to form an oxoiron(IV) ligand field band (λ_{max} = 753 nm, ϵ = 280 M^{-1} cm^{-1}); with this red-shifted LMCT, no isosbestic points

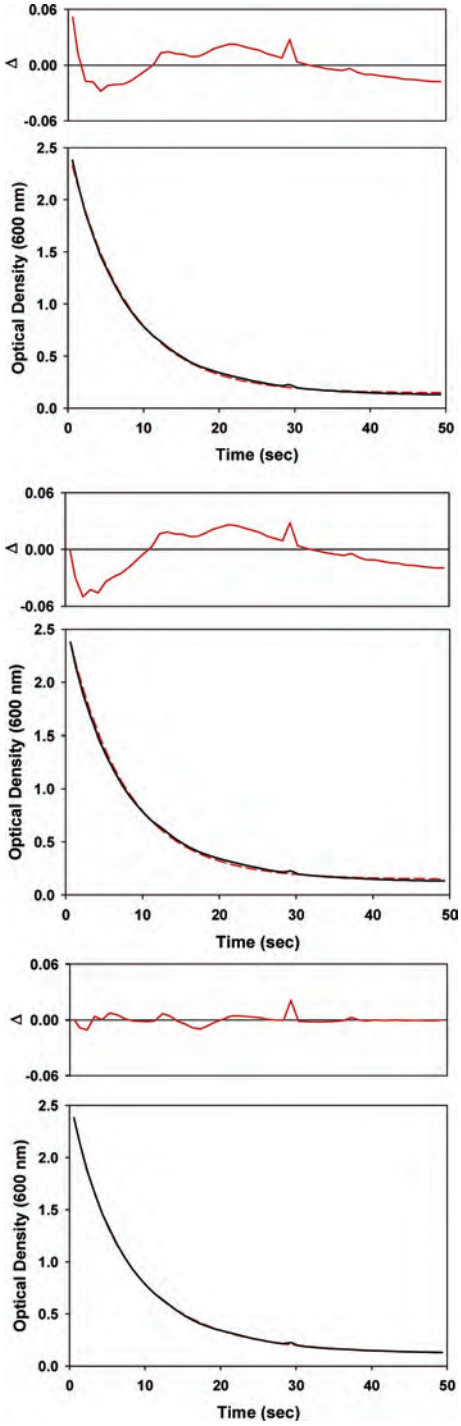

Figure 5. Observed (black) and calculated (red) optical densities at 600 nm calculated using a single wavelength exponential (top), a global A → B model (middle), and a global A → C, B → C model (bottom) for decomposition of the (alkylperoxo)iron(III) intermediate supported by TPA to oxoiron(IV) in CH_3CN in the presence of pyridine *N*-oxide at 231 K (data shown in Figure 4).

were evident. A single wavelength trace coincident with the LMCT maximum deviated from a simple exponential (Figure 8). Again, the data were successfully fit to a parallel (A → C, B → C) reaction scheme (Figures S21 and S22 in Supporting Information), with k_{obs} = 7.88(8) × 10^{-3} s^{-1}, 9.2(1) × 10^{-4} s^{-1} (Figure 9).

Decay of [Fe^{III}(β-BPMCN)(OO^tBu)]$^{2+}$ in CH_2Cl_2. The (alkylperoxo)iron(III) intermediate of β-BPMCN in CH_2Cl_2

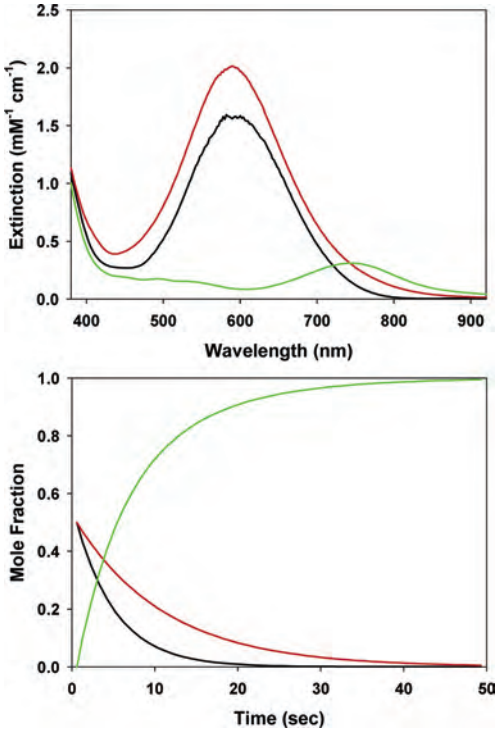

Figure 6. Calculated spectra (top) and time-dependent concentrations (bottom) for A → C, B → C kinetic model of time-dependent optical data shown in Figure 4 for conversion of the (alkylperoxo)iron(III) intermediate supported by TPA to oxoiron(IV) in CH_3CN with added pyridine *N*-oxide, with initial mole fractions arbitrarily set to $[A]_0 = 0.50$, $[B]_0 = 0.50$, and $[C]_0 = 0$.

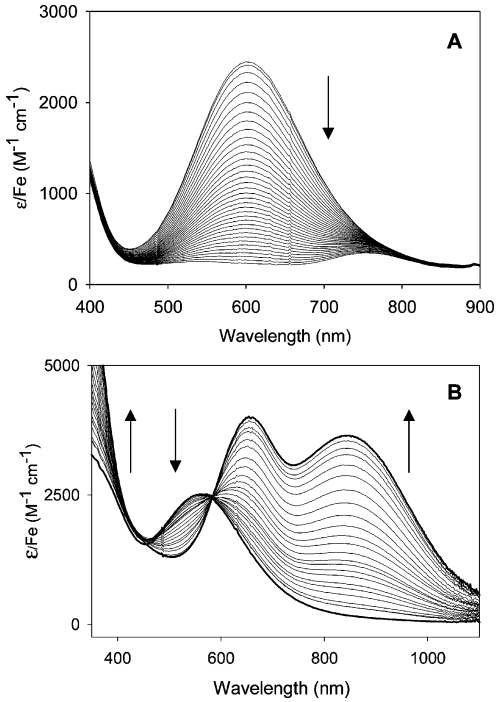

Figure 7. Time-dependent evolution of visible−NIR spectra for decomposition of the (alkylperoxo)iron(III) intermediates supported by β-BPMCN to oxoiron(IV) in CH_3CN/H_2O at 228 K (A; $[Fe^{II}]_0 = 0.58$ mM, $[^tBuOOH]_0 = 1.2$ mM, $[H_2O] = 0.3$ M) and to (alkylperoxo)iron(IV) in CH_2Cl_2 at 206 K (B; $[Fe^{II}]_0 = 1.8$ mM, $[^tBuOOH]_0 = 9.0$ mM), as monitored by visible−NIR spectroscopy.

exhibited a distinct purple chromophore ($\lambda_{max} = 566$ nm, $\epsilon = 2500$ M^{-1} cm^{-1}, Figure 7B) at 206 K, and bleaching of

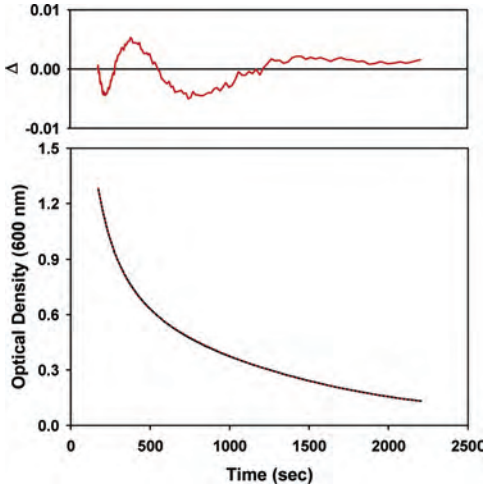

Figure 8. Observed (black) vs calculated (red) optical density at 600 nm for conversion of (alkylperoxo)iron(III) intermediate supported by β-BPMCN to oxoiron(IV) in CH_3CN/H_2O at 228 K for data shown in Figure 7A.

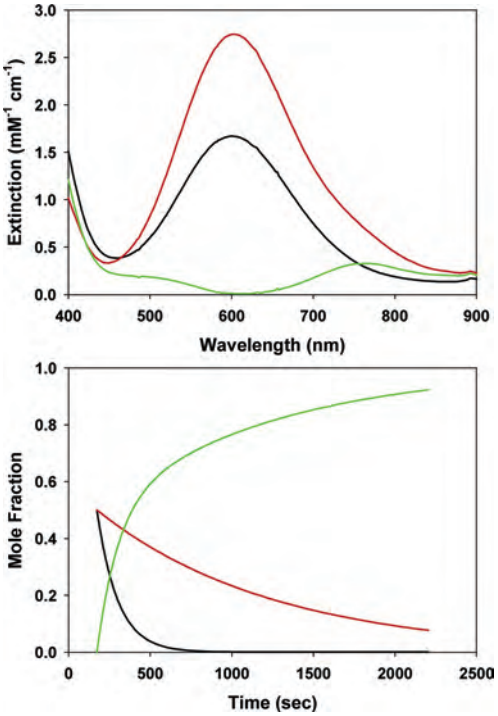

Figure 9. Calculated spectra (top) and time-dependent concentrations (bottom) for A → C, B → C kinetic model for decomposition of the (alkylperoxo)iron(III) intermediate supported by β-BPMCN to oxoiron(IV) in CH_3CN/H_2O at 228 K, with initial mole fractions arbitrarily set to $[A]_0 = 0.50$, $[B]_0 = 0.50$, and $[C]_0 = 0$.

this chromophore produced a unique product spectrum ($\lambda_{max} = 656$, 845 nm; $\epsilon = 4000$, 3600 M^{-1} cm^{-1}) that could not be assigned to an oxoiron(IV) complex. Raman and NMR spectroscopy were consistent with the presence of an alkylperoxo ligand, and hence the product was assigned as an unprecedented (hydroxo)(alkylperoxo)iron(IV) complex;[15] this product formulation is equivalent to a ^{t}BuOOH adduct of an oxoiron(IV) complex. The time course of this reaction was most obvious at long wavelength, where the distinctive product bands dominate the spectrum; the reaction kinetics were biphasic at 840 nm, with a brief induction period

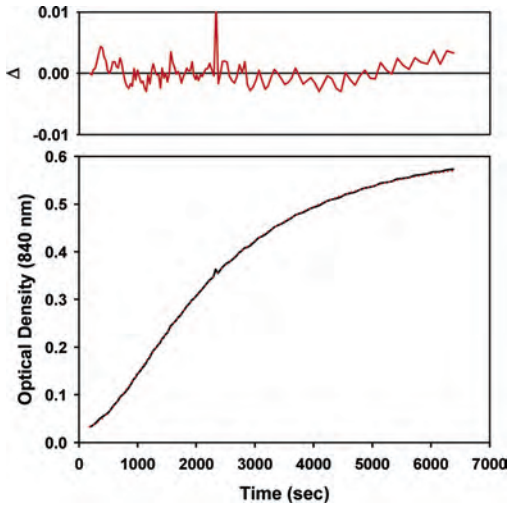

Figure 10. Observed (black) vs calculated (red) optical density at 840 nm for conversion of (alkylperoxo)iron(III) intermediate supported by β-BPMCN to an (hydroxo)(alkylperoxo)iron(IV) product at 206 K for data shown in Figure 7B (path length = 0.1 cm).

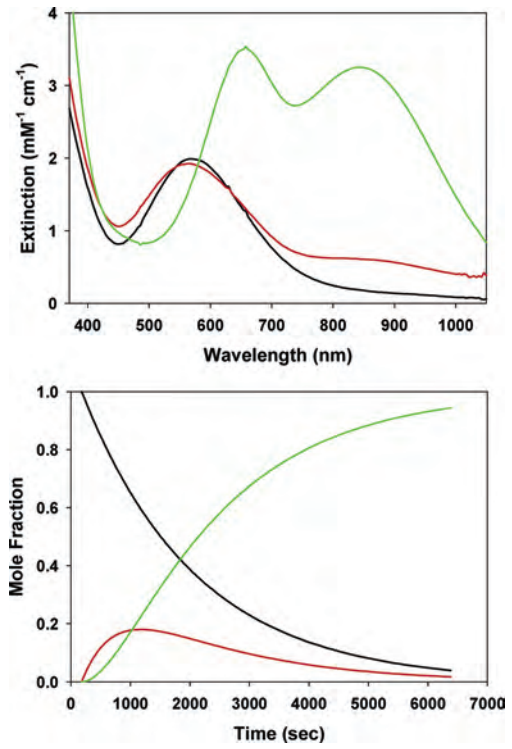

Figure 11. Calculated spectra (top) and time-dependent concentrations (bottom) for an A → B → C kinetic model to the time-dependent optical data shown in Figure 7B for decomposition of the (alkylperoxo)iron(III) intermediate supported by β-BPMCN in CH_2Cl_2 at 206 K.

preceding first-order growth of the product chromophore (Figure 10). Furthermore, the optical data failed to exhibit clean isosbestic points throughout the reaction, clearly indicating the presence of at least one intermediate. The time-dependent optical data were accordingly fit using global least-squares techniques to a scheme of consecutive first-order reactions, A → B → C (k_{obs} = 1.73(6) × 10^{-3} s^{-1}, 5.22(7) × 10^{-4} s^{-1}, Figure 11 and Figures S23 and S24 in Supporting Information). The two rate constants from the kinetic analysis of data obtained at −67 °C were found to be independent of the starting iron concentration used (0.07−0.33 mM, Table S1), supporting the validity of eq 4 for this transformation. The order of the two calculated rate constants could not be determined, as plausible spectra for the intermediate ("B") were calculated for either permutation. In fact, both calculated spectra for B retained a significant CT band only slightly blue-shifted from the initial chromophore, suggesting that the intermediate is a distinct (alkylperoxo)iron(III) complex.

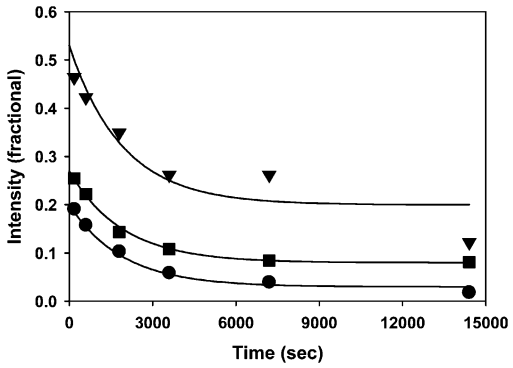

Figure 12. Time course for decay of the three EPR signals associated with the (alkylperoxo)iron(III) intermediate supported by β-BPMCN in CH_2Cl_2 at 206 K ($[Fe^{II}]_0$ = 1.0 mM, $[^tBuOOH]_0$ = 10 mM; circle, g = 2.2; square, g = 4.3; triangle, g = 8). Exponentials correspond to the slower observed rate constant of 5.2 × 10^{-4} s^{-1} obtained from the A → B → C kinetic model fit to optical data (Figure 11).

The reaction was monitored independently at −67 °C by periodically freeze-quenching aliquots into EPR tubes (Figure 12). Three different signals (g = 1.96−2.18, g = 4.3, g = 8) corresponding to an 86% yield of spin-isomeric (alkylperoxo)iron(III) species were observed;[15] their monotonic decay to EPR-silent iron(IV) product paralleled a single-exponential corresponding to the slower rate determined optically under comparable conditions (Figure 12). Because the brief induction period was not resolved in this time course, a more detailed analysis was not warranted, notwithstanding the more complex kinetic model applied to the optical data. Qualitative monitoring of the reaction by resonance Raman spectroscopy revealed only minor initial changes in the (alkylperoxo)iron(III) ν(O−O) modes, followed by their subsequent decay.

Finally, the rates of reaction of all the (alkylperoxo)iron(III) complex intermediates to iron(IV) species were determined over a range of experimentally accessible temperatures (Table S1 in Supporting Information). Arrhenius plots are shown in Figure 13, and derived activation parameters are collected in Table 3. The temperature dependences are all very similar, except for that of the slower observed rate for decay of the (alkylperoxo)iron(III) intermediate supported by β-BPMCN in CH_2Cl_2, which forms the unique (alkylperoxo)iron(IV) product. Its smaller slope compared to the others suggests a different chemical transformation from that associated with the other reactions. Most importantly, the applied kinetic models are robust over a wide range of temperatures and observed rates.

4. Discussion

This study has examined the decomposition of low-spin (alkylperoxo)iron(III) intermediates supported by the three

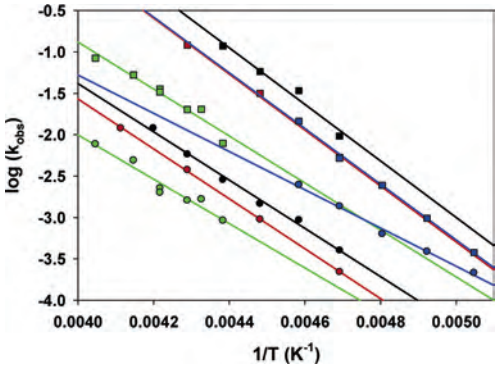

Figure 13. Arrhenius plots for the decay reactions of (alkylperoxo)iron(III) intermediates to iron(IV) products for the following ligands and solvents: TPA/acetone (red); 5-Me$_3$TPA/acetone (black); β-BPMCN/CH_3CN/H_2O (green); β-BPMCN/CH_2Cl_2 (blue).

Table 3. Observed Temperature Dependence for Reaction Steps Forming Iron(IV) Species

ligand, solvent	R^2	$\Delta H^{\ddagger}_{obs}$, kJ/mol	$\Delta S^{\ddagger}_{obs}$, J/(mol K)	ref
5Me$_3$TPA, acetone				
k_1	0.970	64(8)	+19(37)	*a*
k_2	0.994	54(2)	−54(10)	
TPA, acetone				
k_1	0.997	63(4)	+9(17)	*a*
k_2	0.999	56(1)	−50(3)	
BPMCN, CH_3CN				
k_1	0.942	52(6)	−51(26)	*a*
k_2	0.941	49(6)	−85(24)	
BPMCN, CH_2Cl_2				
k_{slow}	0.998	42(2)	−98(11)	*a*
k_{fast}	0.993	63(2)	+9(9)	
TPA, CH_3CN/PyNO		52(1)	−74(3)	38
TPA, acetone/H_2O_2		54(3)	−39(12)	49

[a] This work.

closely related tetradentate nonheme ligands shown in Chart 1 to metastable iron(IV) products. The study included reactions in several solvents, so that the sixth solvento ligand site was also varied. The (alkylperoxo)iron(III) intermediates were formed in situ by rapid oxidation of iron(II) complexes with excess ^{t}BuOOH; this process is essentially quantitative in CH_3CN and CH_2Cl_2 but somewhat less efficient in acetone, particularly at higher temperatures. Subsequent decomposition reactions involve O−O bond homolysis to form oxoiron(IV) complexes in three cases and a distinct (alkylperoxo)iron(IV) species in the case of the β-BPMCN complex in CH_2Cl_2. One plausible interpretation of the results would associate all observed reaction rates with $Fe^{III}O-OR$ bond homolyses of (alkylperoxo)iron(III) complex intermediates, except for the distinctive slower rate for β-BPMCN in CH_2Cl_2, which might reflect a different sort of transformation (vide infra).

An unexpected complication was the general observation of biphasic kinetics for the conversion of (alkylperoxo)iron(III) intermediates to oxoiron(IV), which was interpreted for all these cases to involve two parallel decay pathways. The most straightforward rationale for this situation would be geometric isomerism of the (alkylperoxo)iron(III) complex, in which the peroxide is coordinated in either of the two inequivalent sites trans to the amine or a pyridine donor of the tetradentate supporting ligand (Chart 1). Isomers decomposing by O−O bond homolysis would yield two distinct first-order traces under the differential trans influence, provided that the low spin state of iron(III) prevented facile interconversion of the isomers on the reaction time scale. The ratio of observed rates is consistent with a modest trans influence, $\Delta\Delta G^{\ddagger} = 2-7$ kJ/mol. DFT calculations on isomers of $[Fe^{III}(TPA)(OH)(OOH)]^+$ suggest the ground-state arrangement of the peroxo ligand trans to the amine would be more stable by only 11 kJ/mol,[58] and a recent DFT study of low-spin (alkylperoxo)iron(III) complexes of a related tetradentate ligand suggest the isomeric Raman spectra would be very similar.[40] Indeed, the presumptive isomers are not obviously resolved in EPR and Raman spectra, so independent corroboration of this hypothesis has not been possible.

Other forms of isomerism might include five- vs six-coordinate species, different solvento coligands, and different spin states. Coincident solvent effects on both observed rates clearly preclude a common five-coordinate species, and significantly different sixth-site ligands might be expected to shift the relative LMCT energies. Moreover, five-coordinate (alkylperoxo)iron(III) complexes are expected to be high-spin, and such species are not observed for the TPA and BPMCN intermediates in MeCN.[48] We also discount the possibility of cis- and trans-folded peroxide ligands; for example, calculations on ^{t}BuOOH predict that the cis structure is coincident with the global maximum of the energy profile for rotation about the O−O bond.[59]

A theoretical study of FeO−OR bond homolysis in hypothetical model complexes $[(H_3N)_4Fe^{III}(OH_x)(OO^tBu)]^{x+}$ ($x = 1, 2$) concluded that a low-spin ($S = 1/2$) ground state facilitates dissociation of the alkoxyl radical and formation of the oxoiron(IV) center.[47,48] The activation barrier was estimated to be 60−80 kJ/mol with minimal entropic contribution. In contrast, a high-spin ($S = 5/2$) state presents a significant orbital barrier to FeO−OR bond homolysis and instead leads to Fe−OOR bond homolysis.[48] Use of the temperature-dependent rates observed in this study to derive experimental activation parameters for O−O bond homolysis may be problematic, given the possibilities of spin and sixth-site ligand equilibria. Notwithstanding the kinetic complexities already described, observed activation enthalpies obtained for decomposition of the various (alkylperoxo)iron(III) intermediates closely approach the theoretical estimate of the activation energy for homolytic O−O bond cleavage in a model low-spin (alkylperoxo)iron(III) complex (Table 3). Hence, we invoke a coincident mechanism of rate-limiting, irreversible O−O bond homolysis for these reactions, eqs 2 and 4, except as noted for the formation of (alkylperoxo)iron(IV) in CH_2Cl_2 (vide infra).

There appears to be a compensation effect within the temperature-dependent rate data, such that increasing activation enthalpies are offset by increasingly positive entropies (Figure 14). Arbitrary fitting of a linear relationship to available data, including the previously reported pyridine *N*-oxide promoted and acetone/H_2O_2 condensate reactions

(58) Bassan, A.; Blomberg, M. R. A.; Siegbahn, P. E. M.; Que, L., Jr. *J. Am. Chem. Soc.* **2002**, *124*, 11056−11063.
(59) Khursan, S. L.; Antonovsky, V. L. *Russ. Chem. Bull., Int. Ed.* **2003**, *52*, 1312−1325; *Izv. Akad. Nauk., Ser. Khim.* **2003**, 1241−1253.

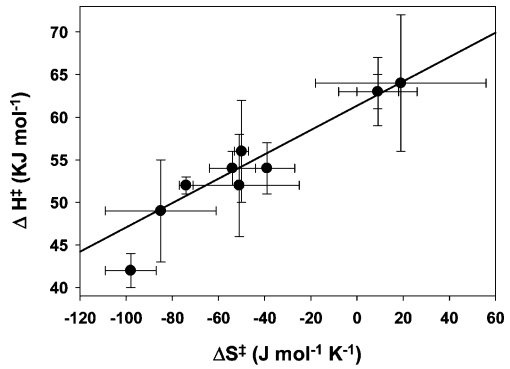

Figure 14. Isokinetic plot for decompositions of (alkylperoxo)iron(III) intermediates.

of TPA complexes,[38,49] yields an isokinetic temperature $\beta = 143 \pm 12$ K and $\Delta H^{\ddagger} = 61.3(6)$ kJ/mol at the intercept. Similar trends reported for metal−alkyl bond homolyses of alkylcobalt(III) complexes were attributed to more product-like transition states resulting from increased endothermicity of the bond homolysis, with concomitantly positive activation entropy.[60] The less compelling range of the postulated trend in this work may reflect the relatively weak O−O bonds and attenuated steric effects on their cleavage. Nevertheless, the negative entropies observed herein are striking for a unimolecular fragmentation.[61,62]

The decomposition of the β-BPMCN-supported (alkylperoxo)iron(III) complex in CH_2Cl_2 (Figure 7B) differs from the other reactions in several respects.[15] First of all, instead of an oxoiron(IV) complex, a unique (hydroxo)(alkylperoxo)-iron(IV) product is formed, which entails the interaction of the iron center with a second equiv of ^{t}BuOOH. Second, the kinetics of its formation exhibits biphasic kinetics that requires a sequential (A → B → C) scheme (rather than a parallel scheme as found for the others), in which the faster step has a rate constant about three times larger than that of the slower step. Third, the faster observed rate has a temperature dependence similar to the other reactions and activation parameters that fit into the line drawn for the isokinetic plot (Figures 13 and 14), but the slower observed rate is distinct and has a smaller activation enthalpy. Given the product formulation for this reaction, the mechanism of product formation likely involves the combination of distinct adduct formation and O−O bond homolysis steps, but our kinetic analysis does not allow the order of the observed rates to be unambiguously established. Therefore, four permutations are possible for assignment of the two observed rate constants to the two mechanistic steps (Scheme 1).

The most straightforward sequence involves initial O−O bond homolysis of the Fe^{III}−OOR intermediate to form an Fe^{IV}═O species followed by 1,2-capture of excess ^{t}BuOOH to form the (hydroxo)(alkylperoxo)iron(IV) product (permutations i and iii in Scheme 1). However, the fact that the calculated spectrum for intermediate B is only slightly shifted from the initial (alkylperoxo)iron(III) chromophore suggests that B is still an (alkylperoxo)iron(III) species and O−O bond cleavage to form an iron(IV) species has not occurred at this stage. Thus, permutations i and iii can be excluded by this argument.

Permutations ii and iv involve initial formation of the Fe^{III}-(OOR)(ROOH) adduct followed by O−O bond homolysis; they differ only in the assignments of the faster and the slower steps. On the assumption that the Fe^{III}(OOR)(ROOH) adduct is the only plausible low-spin iron(III) species that can form in CH_2Cl_2 solution, the observation that the low-spin iron(III) species represents only a small fraction (20%) of the iron(III) species present in both EPR and Raman spectra is inconsistent with permutation iv where the adduct

Scheme 1

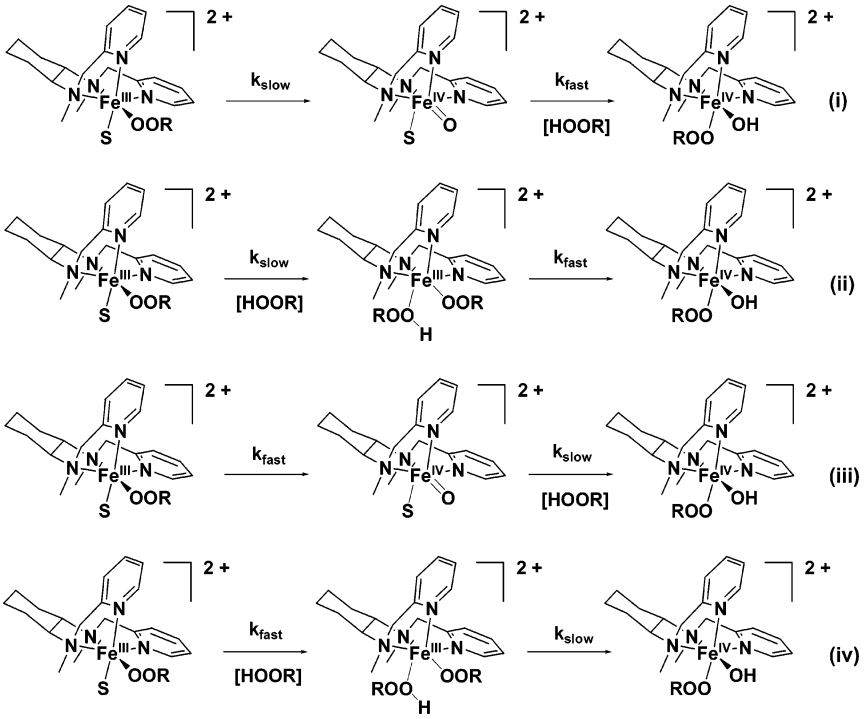

would be expected to accumulate and become the major component. Furthermore the EPR time course clearly shows the simultaneous decay of both high-spin and low-spin iron(III) signals to silent oxoiron(IV) species with the same slow rate constant (Figure 12), which is inconsistent with permutation iv. On the other hand, the temperature dependence of the faster step matches those of the other transformations discussed in this paper, supporting its assignment to the O−O bond homolysis step, as in permutation ii. This leads to the assignment of the adduct formation step to the slower observed rate, which has the more negative entropy of activation that would be associated with a bimolecular reaction. Taken together, these arguments favor assignment of permutation ii, in which a slow initial step forms an Fe^{III}(OOR)(ROOH) adduct, presumably including spin crossover to a reactive low-spin state that subsequently forms a (alkylhydroperoxide)oxoiron(IV) complex by O−O bond homolysis at the faster observed rate, with final, rapid tautomerization to the final (hydroxo)(alkylperoxo)iron(IV) product.

Two problems remain unresolved regarding this mechanistic assignment. First, the fast observed rate assigned to (alkylperoxo)iron(III) homolysis should also exhibit complications of geometric isomerism, but the reaction kinetics are fit well by sequential single exponentials. Unlike the (alkylperoxo)iron(III) intermediates, clear spectroscopic evidence for isomerism was obtained for the (alkylperoxo)iron(IV) product: two distinct, paramagnetically shifted ^{2}H NMR signals were observed in a 60:40 ratio for the product derived from a reaction using $(CD_3)_3COOH$, and two sets of Raman modes exhibited different excitations using 632.8 and 752.5 nm laser irradiation.[15] There are two possible explanations for this discrepancy. First, the iron(IV) isomers might indeed form by overlapping reactions of (alkylperoxo)iron(III) isomers, but the isomeric rates might be accidentally degenerate, as for the TPA-supported intermediate in the presence of pyridine *N*-oxide. Second, rapid tautomerization within the Fe^{III}(OOR)(ROOH) adduct would give exclusive reaction by the faster isomer, but the iron(IV) product might be configurationally unstable on the reaction time scale. A second issue is whether a [^{t}BuOOH] dependence can be observed for the slower observed rate assigned to adduct formation. Bimolecular adduct formation should exhibit first-order dependence but not the reverse unimolecular dissociation, spin crossover, or subsequent homolysis step. Therefore, the kinetic dependence on [^{t}BuOOH] will fall between zero- and first-order limits. Unfortunately, time-dependent concentrations of alkylhydroperoxide could not be determined, and the large, 5- to 10-fold stoichiometric excess of ^{t}BuOOH required to obtain full accumulation of the (alkylperoxo)iron(III) and (alkylperoxo)iron(IV) chromophores did not allow an experimental dependence on [^{t}BuOOH] to be established for phases subsequent to the initial iron(II) oxidation.

Despite the significant remaining mechanistic uncertainties regarding formation of the (alkylperoxo)iron(IV) complex, a close relationship to formation of the other oxoiron(IV) products is clearly demonstrated, as the limiting rates of O−O bond homolyses leading to the disparate products are nearly coincident. Moreover, the overall kinetic data further substantiate the influence of the supporting ligation on the rate of O−O bond homolysis. Observed rates are clearly affected by the supporting and solvento ligands, as the combined kinetic effects exceed 2 orders of magnitude. Thus, the 5-Me_3TPA reaction is slightly faster than the TPA reaction in acetone, and the reaction in CH_3CN promoted by pyridine *N*-oxide is faster still. The β-BPMCN reaction is relatively slow in CH_3CN/H_2O but matches the TPA/acetone rate in CH_2Cl_2, despite the formation of divergent iron(IV) products. Notwithstanding the unanticipated complexity in the observed kinetics, the experimental observations substantiate earlier theoretical calculations that predicted the observed enthalpic barrier to O−O bond homolyses of low-spin (alkylperoxo)iron(III) intermediates[46,47] while further elucidating an unexpectedly rich reaction landscape.

Acknowledgment. This work was supported by the National Institutes of Health (Grants GM-33162 and GM-38767 to L.Q. and Grant EB-001475 to E.M.). M.C. thanks Fundacio La Caixa for a postdoctoral fellowship, and A.S. thanks the National Science Foundation for a Graduate Research Fellowship.

Supporting Information Available: Kinetic data, resonance Raman and EPR spectra of TPA and 5-Me_3TPA (alkylperoxo)iron(III) intermediates in frozen acetone, and details of the kinetic fits. This material is available free of charge via the Internet at http://pubs.acs.org.

IC0607787

(60) Halpern, J. *Bull. Chem. Soc. Jpn.* **1988**, *61*, 13−15.
(61) Huang, K.-W.; Han, J. H.; Cole, A. P.; Musgrave, C. B.; Waymouth, R. M. *J. Am. Chem. Soc.* **2005**, *127*, 3807−3816.
(62) DiPasquale, A. G.; Hrovat, D. A.; Mayer, J. M. *Organometallics* **2006**, *25*, 915−924.